

The In-Flight Realtime Trigger and Localization Software of GECAM

Xiao-Yun Zhao¹, Shao-Lin Xiong¹, Xiang-Yang Wen¹, Xin-Qiao Li¹, Ce Cai¹,², Shuo Xiao¹,², Qi Luo¹,², Wen-Xi Peng¹, Dong-Ya Guo¹, Zheng-Hua An¹, Ke Gong¹, Jin-Yuan Liao¹, Yan-Qiu Zhang¹, Yue Huang¹, Lu Li¹, Xing Wen¹, Fei Zhang¹, Jing Duan¹,², Chen-Wei Wang², Dong-Li Shi¹,³, Peng Zhang¹,³, Qi-Bin Yi¹,⁴, Chao-Yang Li¹,⁵, Yan-Bing Xu¹, Xiao-Hua Liang¹, Ya-Qing Liu¹, Da-Li Zhang¹, Xi-Lei Sun¹, Fan Zhang¹, Gang Chen¹, Huan-Yu Wang¹, Sheng Yang¹, Xiao-Jing Liu¹, Min Gao¹, Mao-Shun Li¹, Jin-Zhou Wang¹, Xing Zhou¹,², Yi Zhao¹,6, Wang-Chen Xue¹,², Chao Zheng¹,², Jia-Cong Liu¹,², Xing-Bo Han², Jin-Ling Qi², Jia Huang², Ke-Ke Zhang², Can Chen¹,², Xiong-Tao Yang¹, Dong-Jie Hou¹, Yu-Sa Wang¹, Rui Qiao¹, Xiang Ma¹, Xiao-Bo Li¹, Ping Wang¹, Xin-Ying Song¹, Li-Ming Song¹, Shi-Jie Zheng¹, Bing Li¹, Hong-Mei Zhang¹, Yue Zhu¹, Wei Chen¹, Jian-Jian He¹, Zhen Zhang¹, Jin Hou³, Hong-Jun Wang³, Yan-Chao Hao³, Xiang-Yu Wang³, Zong-Yuan Yang³, Zhi-Long Wen³, Zhi Chang¹, Yuan-Yuan Du¹, Rui Gao¹, Xiao-Fei Lan⁵, Yan-Guo Li¹, Gang Li¹, Xu-Fang Li¹, Fang-Jun Lu¹, Hong Lu¹, Bin Meng¹, Feng Shi¹, Hui Wang¹, Hui-Zhen Wang¹, Yu-Peng Xu¹, Jia-Wei Yang¹, Xue-Juan Yang⁴, Shuang-Nan Zhang¹, Chao-Yue Zhang², Cheng-Mo Zhang¹, Zhi-Cheng Tang¹, and Cheng Cheng² Key Laboratory of Particle Astrophysics, Institute of High Energy Physics, Chinese Academy of Sciences, Beijing 100049, China; xiongsl@ihep.ac.cn,

wenxy@ihep.ac.cn, lixq@ihep.ac.cn

² University of Chinese Academy of Sciences, Chinese Academy of Sciences, Beijing 100049, China

³ School of Information Science and Technology, Southwest Jiaotong University, Chengdu 611756, China

⁴ Key Laboratory of Stellar and Interstellar Physics and Department of Physics, Xiangtan University, Xiangtan 411105, China

⁵ Physics and Space Science College, China West Normal University, Nanchong 637002, China

⁶ Department of Astronomy, Beijing Normal University, Beijing 100875, China

⁷ Innovation Academy for Microsatellites of CAS, Shanghai 201203, China

⁸ Changchun University of Science and Technology, Changchun 130022, China

⁹ Chinese Academy of Sciences South America Center for Astronomy, National Astronomical Observatories, CAS, Beijing 100101, China Received 2022 April 29; revised 2023 June 5; accepted 2023 June 29; published 2024 September 3

Abstract

Realtime trigger and localization of bursts are the key functions of GECAM, an all-sky gamma-ray monitor launched on 2020 December 10. We developed a multifunctional trigger and localization software operating in the CPU of the GECAM Electronic Box. This onboard software has the following features: high trigger efficiency for real celestial bursts with a suppression of false triggers caused by charged particle bursts and background fluctuation, dedicated localization algorithm optimized for both short and long bursts, and low time latency of the trigger information which is downlinked through the Global Short Message Communication service of the global BeiDou navigation system. This paper provides a detailed description of the design and development of the trigger and localization software system for GECAM. It covers the general design, workflow, the main functions, and the algorithms used in the system. The paper also includes on-ground trigger tests using simulated gamma-ray bursts generated by a dedicated X-ray tube, as well as an overview of the performance for real celestial bursts during its in-orbit operation.

Key words: telescopes – instrumentation: detectors – methods: observational

1. Introduction

The Gravitational wave high-energy Electromagnetic Counterpart All-sky Monitor (GECAM) is a constellation of twin micro-satellites (Xiong 2017, unpublished) designed for all-sky monitoring of gamma-ray transients, including gamma-ray bursts (GRBs), particularly those associated with gravitational wave (GW) events and high energy neutrinos (HENs), magnetar bursts (SGRs), X-ray binaries (XRBs), solar flares (SFLs), terrestrial gamma-ray flashes (TGFs) and terrestrial electron beams (TEBs).

On 2020 December 10 (Beijing time), both GECAM satellites were launched to the same orbit with an inclination of

approximately 29° and a height of 600 km (HAN et al. 2020). These two satellites do not have direct communication while in orbit. As illustrated in Figure 1, each GECAM satellite contains a detector dome and an Electronic Box (EBox) as its payload. The energy range of the bursts that each satellite can monitor covers the entire unblocked sky region from about 10 keV to 5 MeV (LI et al. 2020). The key information of those bursts that are triggered and located in real time will be downlinked to the ground with the Global Short Message Communication (GSMC) service of the BeiDou navigation system (BDS-3; Li et al. 2021), which will facilitate joint and follow-up observations with multimessenger and multi-wavelength telescopes.

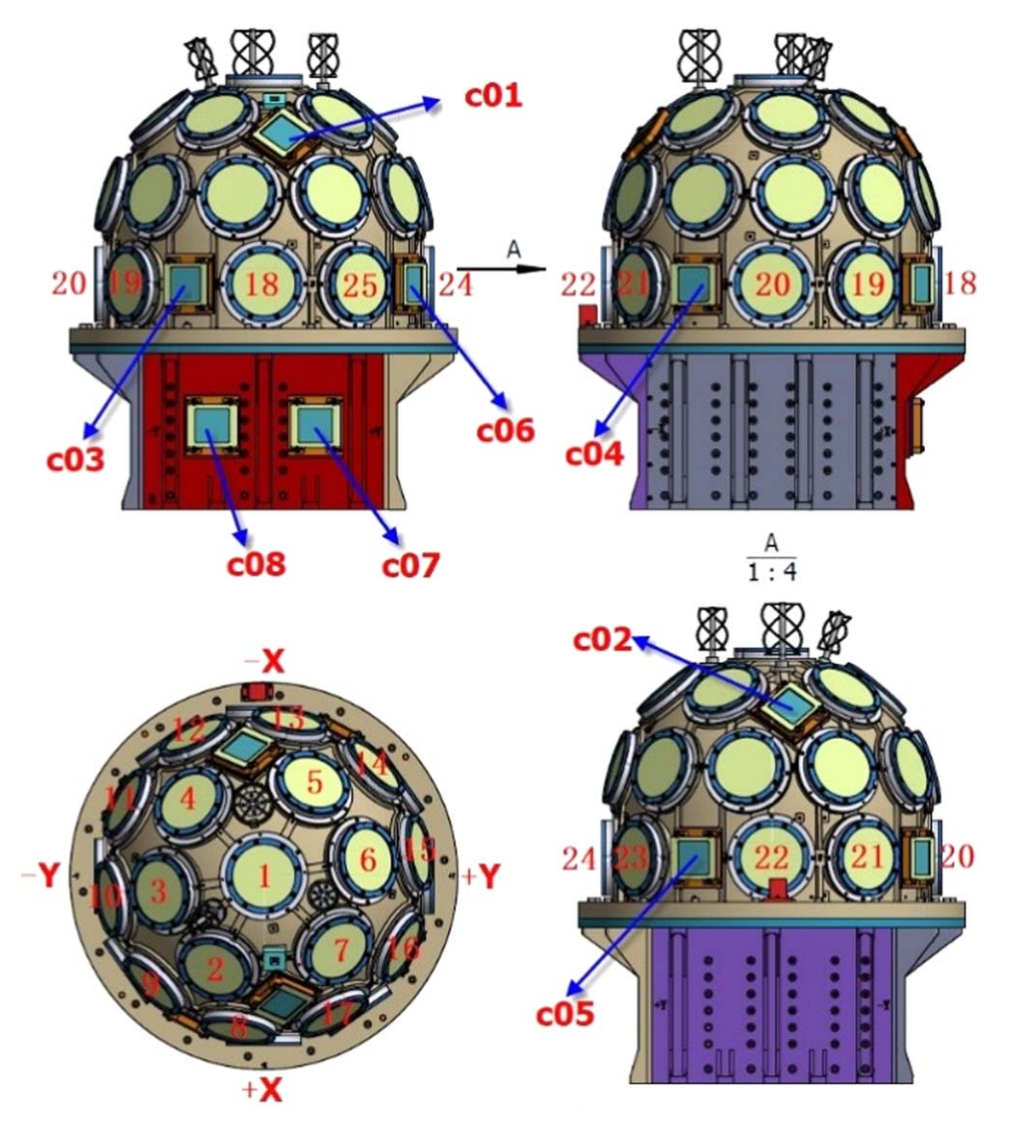


Figure 1. Schematic diagram of the GECAM payload which consists of a detector dome and an EBox. Different views of the payload are shown together with the payload coordinate system illustrated in the bottom left panel; 25 GRDs are displayed with numbers from 1 to 25, while CPDs are labeled starting with "c." Two CPDs are installed in the +X direction of the EBox.

Each GECAM satellite is equipped with 25 Gamma-Ray Detectors (GRDs) (Lv et al. 2018; Zhang et al. 2019; An et al. 2022) and 8 Charged Particle Detectors (CPDs) (Li et al. 2022; Xu et al. 2022; Zhang et al. 2022). All 25 GRDs and 6 CPDs are assembled in the detector dome of the satellite, but with different orientations to cover most of the sky region. Additionally two CPDs are installed in the +X direction of EBox (see Figure 1). The EBox comprises one power supply board, five data acquisition boards, and one data management board with co-running embedded software. It can supply secondary power from the spacecraft to the payload, process scientific and engineering data from detectors, and handle

command and data communication between the payload and spacecraft (LI et al. 2020).

Realtime trigger and localization of bursts, mostly GRBs and SGRs, are crucial for the multi-wavelength and multi-messenger observations. However, among current GRB missions, only Fermi/GBM (Meegan et al. 2009), Swift/BAT (Gehrels et al. 2004), INTEGRAL/IBIS (Mereghetti et al. 2003) and GECAM can provide realtime trigger and localization, with location accuracies of about several degrees for Fermi/GBM, 3'-4' for Swift/BAT and 2'-3' for INT-EGRAL/IBIS. CALET/GBM (Marrocchesi 2018) can provide realtime trigger but without localization. AstroSat/CZTI can

provide trigger (Sharma et al. 2021) and coarse localization (Rao et al. 2016; Saraogi et al. 2022), but the trigger is not for realtime operation. Konus-Wind (Aptekar et al. 1995) and Insight-HXMT/HE (Zhang et al. 2020) can only provide trigger with time latency up to hours or days. The IPN (Hurley et al. 2013), composed of basically all GRB missions, can usually offer good localization but with significant time latency up to several days. The upcoming missions, such as SVOM/ECLAIRs (Godet et al. 2014), SVOM/GRM (Dong et al. 2010), and EP/WXT (Yuan et al. 2018), are designed to have realtime trigger and localization capability.

As the first Chinese space telescope with realtime downlink capability, GECAM is designed to provide realtime triggering and localization of high energy bursts. Therefore, dedicated onboard software for GECAM has been developed, which is configured and executed on the ARM Microcontroller Unit (SAMV71Q21RT-DHB-SV) of the GECAM EBox. This paper presents the detailed design and development of this software system.

2. Software Design

2.1. Requirements

Based on the scientific requirements of GECAM and lessons learned from previous GRB missions, we have defined the following requirements for this GECAM in-flight software:

- (1) The software must continuously evaluate triggers in multiple timescales and energy channel ranges and calculate localization for successful triggers.
- (2) Triggers must be classified into Type I (important triggers, such as GRBs and magnetar bursts) or Type II (other triggers, such as particle events), and generate alert data downlinked via the GSMC service for Type I triggers and only engineering data (without realtime downlink) for Type II triggers.
- (3) The software must generate high time resolution light curves for a short trigger (the main candidate for GW electromagnetic counterpart), which is necessary for on-ground time-delay localization with multiple spacecraft (Xiao et al. 2021). For long triggers, it should generate a count spectrum and light curve spanning about 235 s, which could be used in the on-ground refined localization (Chen et al. 2020).
- (4) The entire software, along with the settings and adjustable parameter tables (trigger parameter tables, localization templates, etc.) can be updated in-flight.

2.2. Overall Design

The trigger and localization software is a part of the GECAM Data Management Unit (DMU) software, which is invoked every 50 ms by the DMU and can be refreshed or re-configured in-flight.

The key functions of this software are illustrated in Figure 2, including background estimation, trigger calculation, localization of event, and light curve generation for a long trigger. To start, it reads the 50 ms time-binned data from the 8 channels of the 25 GRDs, which are obtained from the event data by the data management FPGA (Liu et al. 2022). Then, it accumulates the background from $T_{\rm BkgBstart}$ to $T_{\rm BkgBend}$. Once ready, the software enters the trigger calculation module, where the background is updated every 50 ms as long as no trigger is detected.

The GECAM trigger algorithm uses seven fixed timescales (TrigBx in Figure 2) that are specified in a trigger parameter table along with time bin phase, trigger energy channels (TrigC), threshold, and flag (enable or disable). The blue lines in Figure 2 represent the seven normally used TrigBs, while the cyan lines correspond to all TrigBs longer than 50 ms with a phase shift of half a bin width, which enables the implementation of a sliding time window. The trigger algorithm module allocates a dedicated memory region for this trigger parameter table, and new data are accumulated based on each of the 64 parameters. When the data are ready, the significance for each GRD is calculated for each group of trigger parameters. Once a given number of detectors (an on-orbit adjustable parameter with a default setting of 3) have net counts significantly above the background, e.g., 4σ , no further trigger calculations are performed, and the software proceeds to the location module.

The location of the event is computed using the net counts of 25 GRDs in the energy range of 4–250 keV, for which the location template is made. The location is performed in the first two or all four preset timescales (denoted as Location Bins, LocB in Figure 2) according to its duration judgement result. The four preset LocBs are as follows: one is the trigger timescale, and the other three are extended by 4 s–TrigB, 10 s–TrigB, and 17 s–TrigB respectively. Then the best LocB and best spectrum are selected (see 3.2), in which the final inflight location is obtained by weighting the three directions with the least chi-square values. The location in the payload coordinate system is then transformed to the celestial coordinate system (J2000) which is used for trigger classification.

For each trigger, the software determines whether it is a Type I or Type II trigger based on various information, including the trigger parameters, location, and the counts ratio between CPDs and GRDs (see 3.3 for details). Events classified as particle events, SFLs, or Earth occultation of known sources are flagged as Type II triggers, while others are classified as Type I triggers.

For Type I triggers, trigger information such as the trigger time T_0 , TrigB, energy range, index, and net spectrum of the three most significant GRDs are generated and stored in the first two BeiDou short messages (see Table 1) with higher priority than other messages of this trigger. These messages are downlinked via the BDS-3 in near realtime. However, the

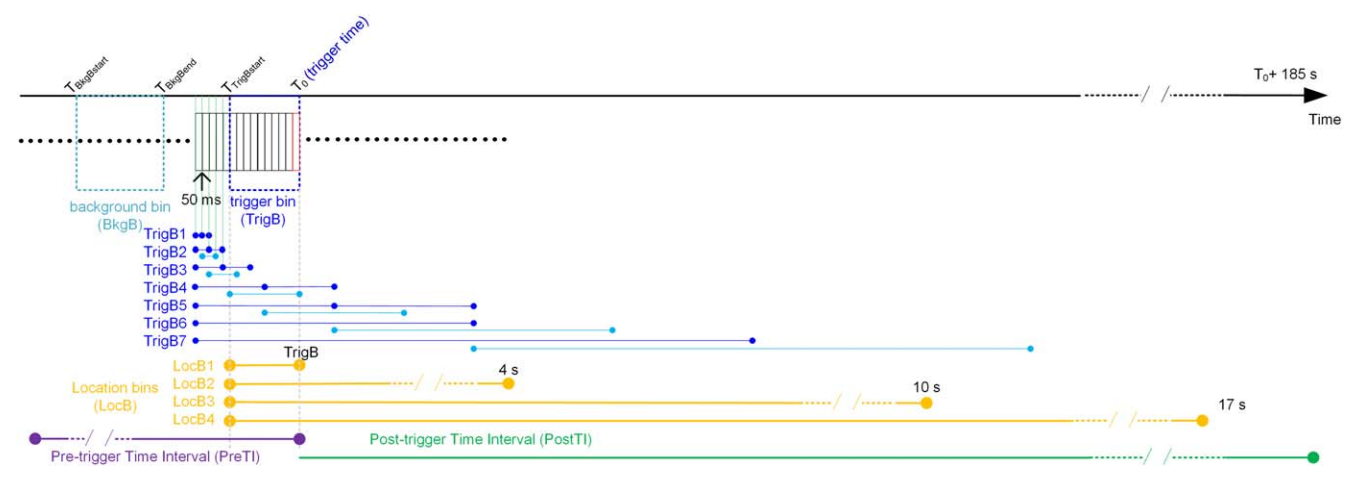


Figure 2. Illustration of the trigger and localization procedures of the GECAM onboard trigger and localization software.

Table 1
The Content of BeiDou Short Messages for Short and Long Triggers

No.	Trigger Type	BDM Index	Format Code	Main Information
1	long trigger (L)	1-2	1	Trigger, location, classification, spectrum of the three most significant GRDs (best location timescale)
2	long trigger (L)	3	2	Light curve of the three most significant GRDs combined
3	long trigger (L)	4	3	Light curve of the three least significant GRDs combined
4	long trigger (L)	5	4	Light curve of eight CPDs combined
5	long trigger (L)	6 - 30	5	Light curve of GRD, one GRD per message
6	long trigger (L)	31	0	Attitude and position of satellite at several given time points
7	short trigger (S)	1-2	1	Trigger, location, classification, spectrum of the three most significant GRDs (best location timescale for short trigger)
8	short trigger (S)	3-4	6	Compression scheme, start time of light curve, high time resolution light curve
9	short trigger (S)	$5 - \leqslant 31$	7	High time resolution light curve

Table 2
The Light Curve Design of the 3rd and 4th Short Messages for the Type I Long
Trigger

Index	TrigB (s)	Total Time of 10 bins Before Trig- ger (s)	Total Time of 18 bins After Trig- ger (s)	Total Time (s)
1	0.05	0.5	0.9	1.4
2	0.1	1	1.8	2.8
3	0.2	2	3.6	5.6
4	0.5	5	9	14
5	1	10	18	28
6	2	20	36	56
7	4	40	72	112

trigger engineering data for Type II triggers will be downlinked via *X*-band rather than BDS-3.

The software also determines whether it is a short trigger or a long trigger based on the significance of the three most significant GRDs in trigger energy range between $T_0 + 2$ s and $T_0 + 4$ s. For Type I and short triggers, the high time resolution

light curve (default bin width of 1 ms) of 25 GRDs within about 2.5 s around T_0 is obtained from the data management FPGA and compressed, because of the limited resources of short messages for each trigger (default of 31 messages per trigger and 70 bytes per message). For Type I and long triggers, the software generates light curves for a duration of $28 \times \text{TrigB}$ seconds in TrigB and within the trigger energy range (TrigE) for both the three most significant and least significant GRDs; Figure 11 provides an example of the light curve for the three most significant GRDs corresponding to index 7 in Table 2. Additionally, light curves of 210 s around T_0 are generated for all CPDs, and light curves of approximately 235 s around T_0 are generated for each GRD.

2.3. Module Design

Figure 3 illustrates the modules for the software and the functions of each module are briefly described below. A detailed implementation of each module is introduced in Section 3.

Energy Channel Selection Module: This module selects data in different specified energy ranges from the time-binned input

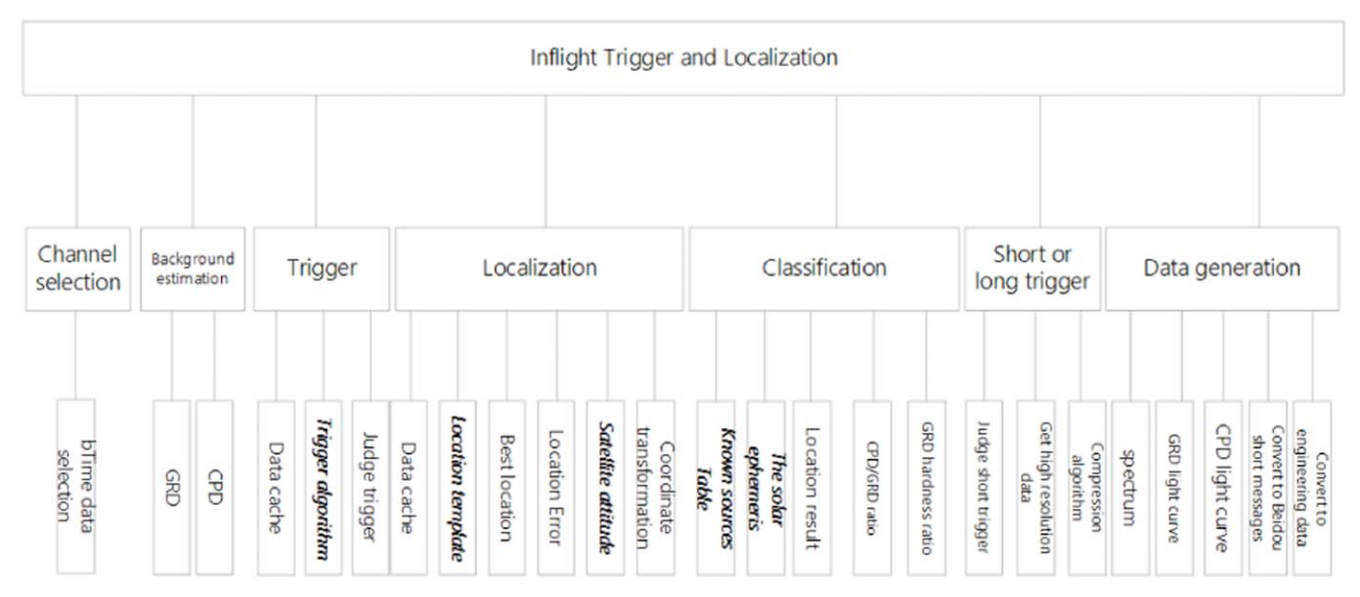


Figure 3. Functional modules of the GECAM onboard trigger and localization software.

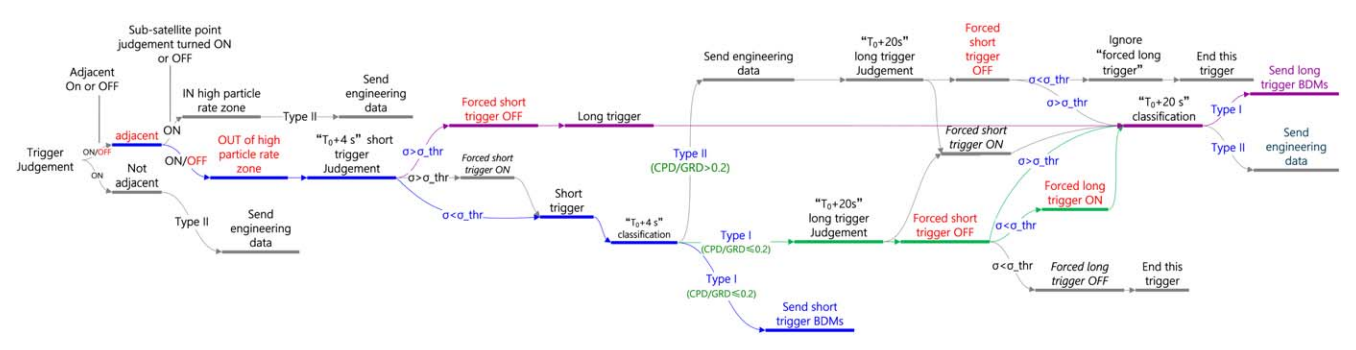


Figure 4. The workflow of the GECAM onboard trigger and localization software.

data (called BTIME data) of 25 GRDs and 8 CPDs every 50 ms. The BTIME data are produced by the data management FPGA, and which represent one of the data types of GECAM. In this data type, the event data are binned into fixed time intervals of 50 ms with 8 channels for each GRD of high gain and low gain. These data serve as the input data type for this software.

Background Estimation Module: This module provides background estimation for both GRDs and CPDs.

Trigger Algorithm Module: This module searches for triggers in realtime based on the input data.

Positioning Module: This module calculates the location of the trigger in J2000 coordinates.

Trigger Classification Module: This module classifies the trigger as either Type I (important events) or Type II (others) based on various criteria.

Short/long Trigger judgement Module: This module judges the coarse duration of the trigger and classifies it as either a short or long trigger. Data Generation Module: This module generates BeiDou short messages for Type I triggers and engineering data for Type II triggers.

2.4. The Workflow

The general workflow of the software is diagrammed in Figure 4. Depending on the combination of different results of short and long trigger judgements, whether "Forced short trigger" or "Forced long trigger" is turned on or off, and the classification result, there can be more than ten branch processes. Among them, the most common processes are the Type I long trigger process, Type I short trigger process, and Type I short and long trigger process, which generate a fixed number of 31, no more than 31, and no more than 62 short messages, respectively. The number of BeiDou short messages for short triggers depends on compression results of the high time resolution light curve.

Figure 4 shows several Flags that control the flow of the software, including "adjacent judgement turned On or OFF," "sub-satellite point judgement turned ON or OFF" (to infer if this trigger is in the high particle rate zone or not), "Forced short trigger" and "Forced long trigger." By default, these Flags are set to OFF, OFF, OFF and ON, respectively.

For a Type I short trigger, it is assumed to be a short trigger for the short trigger judgement at $T_0 + 4$ s, because the signalto-noise ratio (SNR) of the three most significant GRDs in time range of $[T_0 + 3 s, T_0 + 4 s]$ is calculated, and none of them is higher than the short trigger threshold (which is set to 3σ by default). For trigger classification at $T_0 + 4 \,\mathrm{s}$, the net counts ratio between the eight CPDs and the three most significant GRDs in the 4 s after T_0 should be lower than 0.2, so the high time resolution light curves containing the possible burst could be accessed from the FPGA of DMU. Then, the key information on this trigger is organized in the format of BDMs, and DMU sends them to the satellite platform with a fixed rate of one message per second. After that, at $T_0 + 20 \,\mathrm{s}$, a long trigger judgement is performed to check whether this is a real short trigger or not. Since the "Forced long trigger" is turned on, the result of this module will always be a long trigger (for Type I short triggers). Then it comes to the " T_0 + 20 s" classification. If it is judged to not be any other type (No. 0, 2, 3, or 4 in Table 7), it is assumed to be a Type I trigger, and long trigger format BDMs will be generated and sent to the satellite platform.

For a Type I long trigger, if the significance of any of the three most significant GRDs in $[T_0+3\,\mathrm{s},\,T_0+4\,\mathrm{s}]$ is higher than the threshold σ_{thr} , it will only undergo trigger classification at " $T_0+20\,\mathrm{s}$," where the net ratio of CPDs and GRDs is below the threshold, the location range is not in the earth shadow, and neither of the known sources from Table 9 is in the location range, or its hardness ratio is not consistent with this trigger. As a result, long trigger BDMs with light curves of each GRD and all CPDs will be generated and sent to the satellite platform.

3. The Algorithm Principle

3.1. Onboard Trigger

The background estimation module calculates the average single-channel counts of GRD and CPD. There are two adjustable parameters: (1) the time duration $(\Delta t_{\rm bg})$ chosen for the background estimation; (2) the time interval $(\Delta t_{\rm p})$ between the background end time and the trigger time. The default values for $\Delta t_{\rm bg}$ and $\Delta t_{\rm p}$ are 20 s and 5 s respectively, which indicate that data between T_0 - 25 s and T_0 - 5 s will be used as background estimation.

In the Trigger Algorithm Module, as depicted in Figure 5, the software accumulates the total counts (denoted as S) of a GRD within the trigger timescale and energy channel according to the trigger parameter table. With the background estimation (denoted as Bg) provided by the Background Estimation

Module, the SNR of the trigger event is computed using Equation (1), as each observation is independent and obeys the Poisson distribution.

$$SNR = \frac{S - \frac{Bg}{\Delta t_{bg}} \times \Delta t_{s}}{\sqrt{(\sqrt{S})^{2} + \left(\frac{\sqrt{Bg}}{\Delta t_{bg}} \times \Delta t_{s}\right)^{2}}},$$
(1)

where $\Delta t_{\rm s}$ denotes trigger timescale, S stands for the total counts received during $\Delta t_{\rm s}$ in one GRD, $\Delta t_{\rm bg}$ is the time range used for background estimation, and Bg is the total counts in $\Delta t_{\rm bg}$.

As shown in Table 3, the TrigBs span from 50 ms to 4 s, and TrigE covers 4-250 keV according to the initial on-orbit version of the EVT-BTIME mapping table. The trigger energy channel (TrigC) is the channel range corresponding to TrigE. The selection of these energy bands is based on simulations, specifically, with eight spectrum models (PL-Soft, COMP-Soft, Band-Soft, Band-Normal, Band-Hard, Blackbody-soft, Blackbody-norm, Blackbody-hard), simulated background, response matrix, etc. The trigger significance of 15 energy bands is calculated for burst incident angle of $\theta = 90^{\circ}$ and $\phi = 0^{\circ}$ in the payload coordinate system. Five energy bands were recommended in descending order of priority. The selection of TrigB is a result of consideration of several factors: it should be an integer multiple of 50 ms; there should not be too many of them because of limited memory; shorter TrigBs are easier to trigger (Cai 2022).

3.2. Onboard Localization

Once successfully triggered, the refresh of the background, trigger calculation related data, and pre-trigger light curve (PreTI in Figure 2) related data will stop, and the software goes to the localization module with the triggered parameters. The memory data corresponding to this specific TrigB and phase cached in the trigger algorithm module can be directly passed to the array of the four LocBs. As the defined trigger time T_0 corresponds to the trailing edge of the TrigB, and LocBs include TrigB, the start time of LocBs is T_0 - TrigB. Due to limited computing resources onboard, we adopt the detector counts distribution method (Jin-Yuan et al. 2020) to derive the location, which is also used by previous gamma-ray monitors. We build the predefined location templates (Guo et al. 2020) with three different spectra (i.e., soft, normal, and hard spectrum in the Band function). Then the chi-square of the measured data is calculated with these model templates on 2 (for short trigger) or 4 (for long trigger) LocBs. Meanwhile, the sum of SNR for the three most significant GRDs of these LocBs is also calculated in the same energy range of the template. The LocB with the highest SNR is suggested as the best LocB, and the template with the minimum chi-square is assumed as the best location spectrum. Then for the best LocB

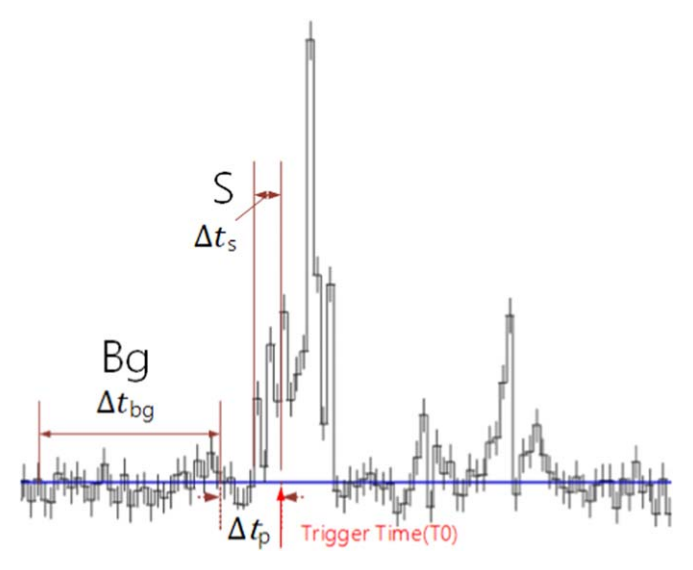


Figure 5. Illustration of the trigger algorithm.

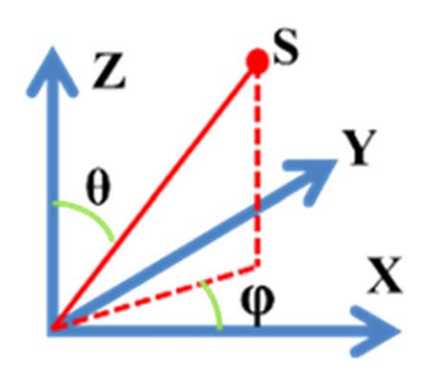


Figure 6. Definition of incident angle (θ, ϕ) of a celestial source (S) in the payload coordinate system.

and the best spectrum, the three incident angles (theta and phi) with the least chi-square values are chosen. The weighted average value of these three sets of theta and phi angles (with $1/\chi^2$ as a weight factor) is the final location in the payload coordinate system for this trigger. This final location result (θ, ϕ) will be transformed to the J2000 coordinate system (R.A., decl.) using the quaternion of the satellite attitude. As drawn in Figure 6, the incident angle θ is the angle between S and +Z, and ϕ is the angle between the projection of S in the XY plane and +X.

The location template is calculated in the payload coordinate system, with a dimension of 3072×26 for each of the three spectra, including the normalized counts and normalization factors (the 26th column) of 25 GRDs for 3072 incident angles. There are four LocBs in total (see Table 4). Except for the first one, which is the triggered TrigB, the other three are all programmable. The values listed in the table are the ones

Table 3 The TrigB and TrigE

TrigB (s)	TrigC	TrigE ^a (keV)
	1-5	8–250
0.05	3-5	25-250
	1-2	8-25
	0 - 1	4–15
	1-5	8–250
	3-5	25-250
0.1, 0.2, 0.5, 1, 2, 4	2-4	15-100
	1-2	8-25
	0-1	4–15

Note.

Table 4
The Timescales for Location Calculation

	-
Index	LocB
1	The triggered TrigB
2	4 s
3	10 s
4	17 s

Table 5
The Classification and its Type

No.	Source Class	Index	Type (adjustable)
0	Known transient source burst	7-99	initial: Type II
1	GRB, SGR, important known transient source	255	initial: Type I
2	Particle event	253	initial: Type II
3	Earth occultation of known sources	101 - 199	initial: Type II
4	SFL	1-5	initial: Type II

retained in flight, where the triggered TrigB is automatically accessed by subsequent modules once triggered. The best LocB will be used to generate light curves and counts spectrum subsequently. The energy range for location is adjustable, and the default setting is $4-250\,\mathrm{keV}$.

3.3. Trigger Classification

The Classification Module aims to classify the nature and origin of the triggered and localized events. The classification for each class of sources is controlled by an adjustable table (see Table 5). By default, events including SFLs, particle events, Earth occultation, or bursts of known sources will be classified as Type II, while all others as Type I.

Classification is performed at $T_0 + 4$ s and $T_0 + 20$ s for short and long triggers, respectively. In the former case (see

^a Based on the initial on-orbit version of EVT-BTIME mapping table.

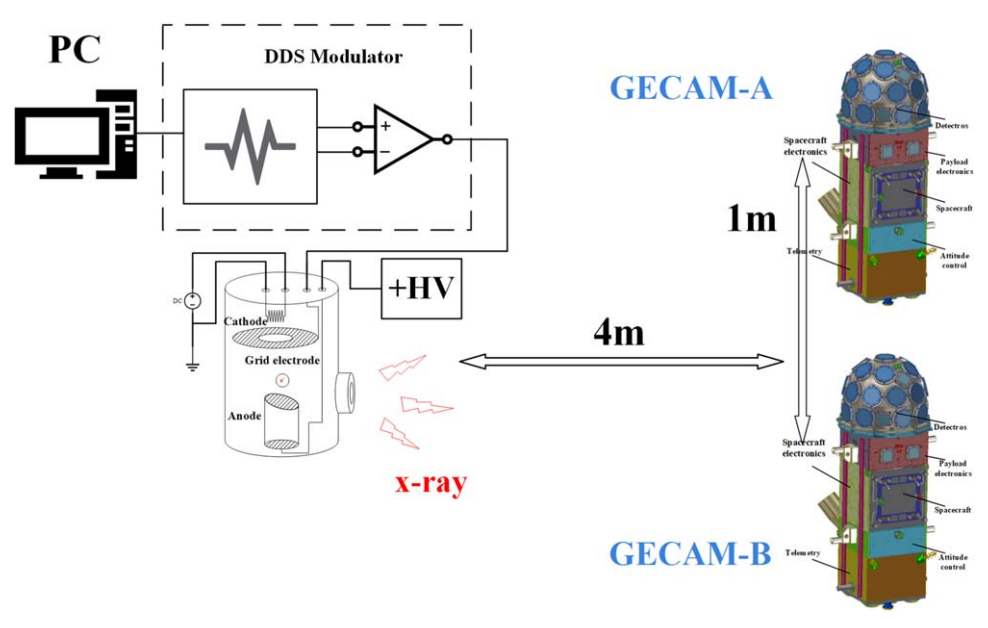


Figure 7. Illustration of the on-ground trigger test for two GECAM satellites before launch.

Table 6 The Classification at $T_0 + 4 \text{ s}$

No.	Classification	Method
0	Particle event	The net ratio of all eight CPDs to the three most significant GRDs in the specific energy range in 4 s after T_0 exceeds the significance threshold
1	GRB, SGR, important known transient source	Not Particle event

Table 7 The Classification at $T_0 + 20$ s

No.	Classification	Method
0	Known transient source burst	Location of this trigger is in the non-shaded areas, the hardness ratio and location of the known source is consistent with that of the trigger
1	GRB, SGR, important known transient source	Not any of other types
2	Particle event	The net ratio of all eight CPDs to the three most significant GRDs in the specific energy range in best Locl exceeds the significance threshold
3	Earth occultation of known sources	Location of this trigger is in the range of occultation edge, the hardness ratio and location of the known sourc is consistent with that of the trigger
4	SFL	Location of this trigger is in the non-shaded areas, the hardness ratio and location of the Sun is consistent with that of the trigger

Table 6), we judge whether the net ratio of all eight CPDs to the three most significant GRDs in the specified energy range in 4 s after T_0 is below the significance threshold $\sigma_{\rm thr}$, (currently set to 0.2). If yes, it is a Type I short trigger, otherwise it is a Type II particle event. For the latter case (see

Table 7), we first use the same method to exclude particle events but with the time bin varied from 4 s to the best LocB. Then we count how many known sources are in the location range. If none, and this location is not in the Earth shadow region, then it will be classified as a Type I long trigger. If

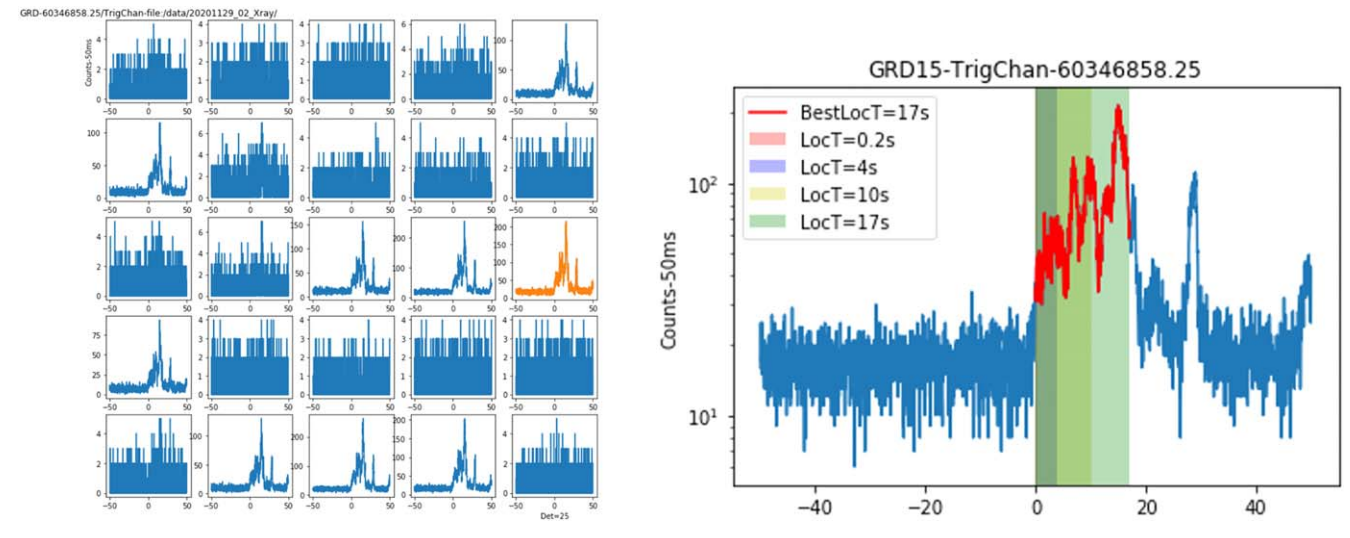


Figure 8. The light curves of the 7th trigger of GECAM-B satellite.

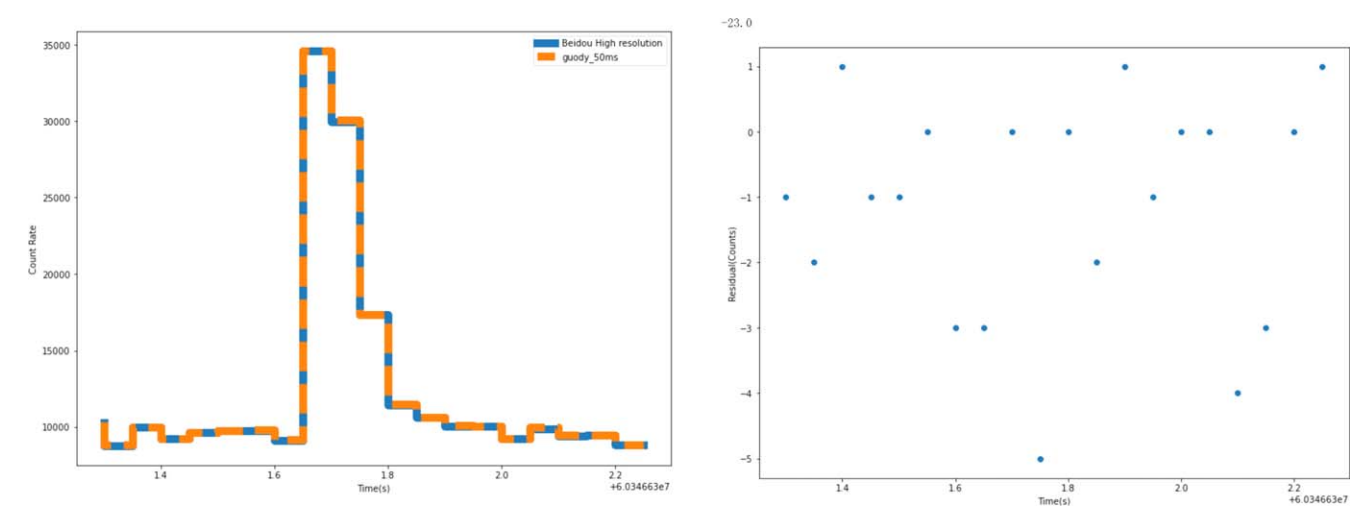


Figure 9. The high time resolution light curve of GECAM-A

none but this location is in the Earth's shadow, then it is assumed as a particle event. Otherwise, further analysis as to whether this location is in the area of occultation edge or out of Earth's shadow region will be carried out. The occultation area in this software is defined as the spherical distance between the trigger location and the pointing direction of the +Z-axis of the payload, which falls within the range of 112° and 115° (adjustable parameter). If the trigger occurs within the occultation area or the non-shaded area, its location and hardness ratio will also be examined to determine if it falls within the corresponding range of the known source, respectively. If yes, it will be assumed to be an occultation or outburst of that source. If none of the above is true, this trigger is labeled as a Type I trigger.

4. On-ground Tests

To test the GECAM onboard trigger and localization software, a series of trigger tests have been done with a portable X-ray tube that can mimic the emission of GRBs (Chen et al. 2021), as illustrated in Figure 7. During the experiment, a total of 15 types of bursts were simulated, including short, long, short, and long burst, etc., and all of them triggered GECAM-A and GECAM-B successfully. Figure 8 displays the light curves of one trigger of GECAM-B. The shadow regions with color indicate the LocBs, and the best LocB (red curve) selected by the software is consistent with offline analysis.

The high time resolution light curve decompressed from BeiDou short messages (blue line) for a short trigger is

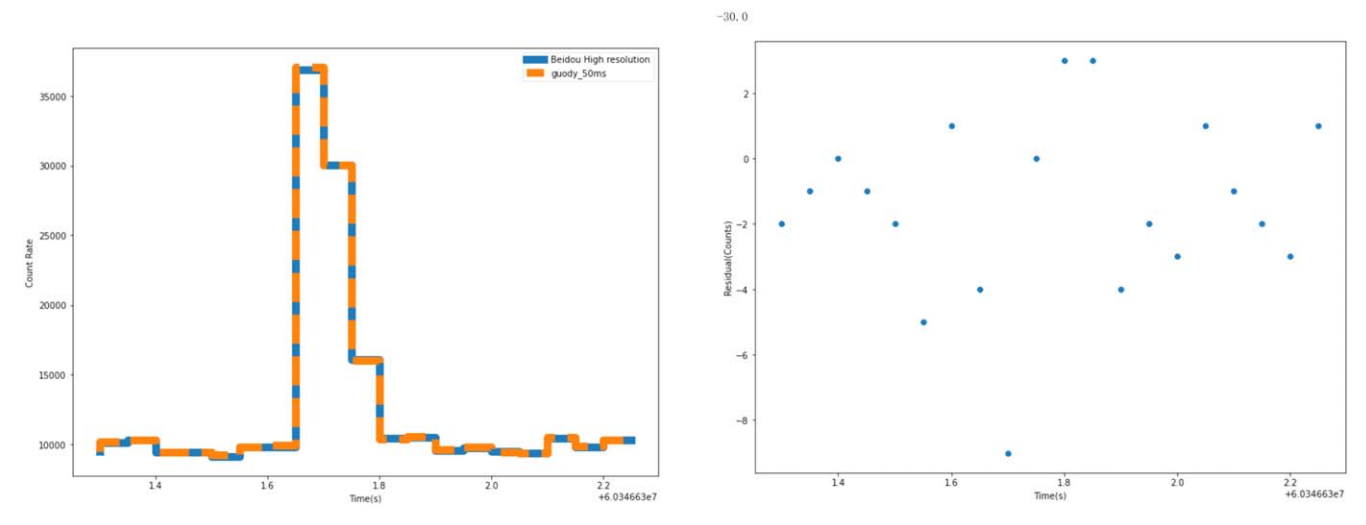


Figure 10. The high time resolution light curve of GECAM-B

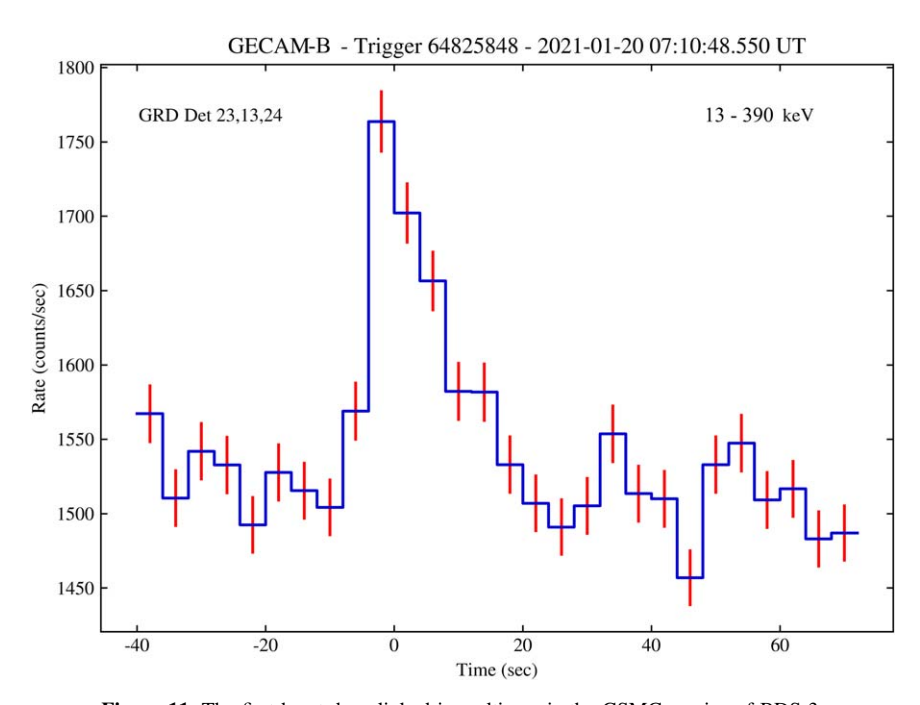
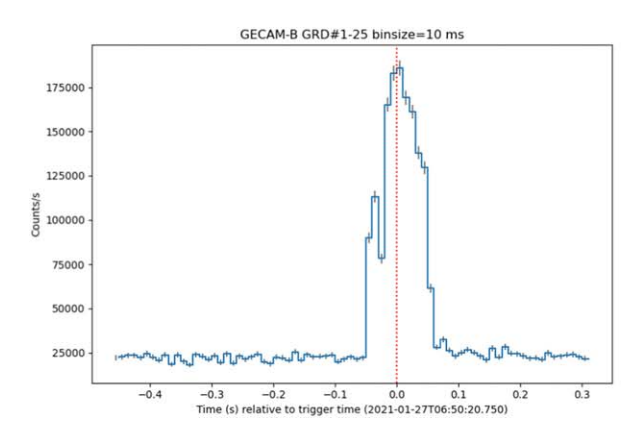


Figure 11. The first burst downlinked in realtime via the GSMC service of BDS-3.

compared to the corresponding 50 ms BTIME data (orange line) as depicted in Figures 9 and 10. The right panel of both figures shows that BDMs are slightly lower than the 50 ms BTIME data. The sum of their residuals (total difference counts) is written in the top left corner of the right panel, -23.0 and -30.0, respectively. The reason is that the high time resolution data of BDMs do not contain energy range boundaries, whereas the BTIME data do.

5. In-flight Tests

Since the launch, GECAM has undergone both Type I and Type II triggers (including GRBs, SGRs, SFLs, and Earth occultation of Sco X-1), and both long and short bursts, confirming that the onboard trigger and localization software work normally. However, due to power supply issues, only GECAM-B was turned on to observe in-flight, so the data presented in this paper come only from GECAM-B. It is



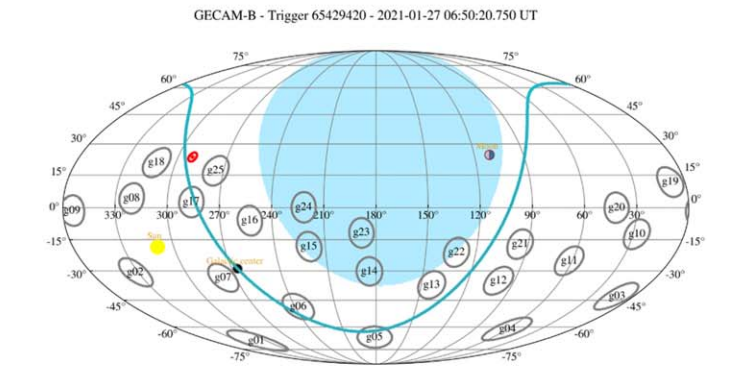


Figure 12. The high time resolution light curve (left panel) and the in-flight localization (right panel) for the first short trigger, which is from SGR J1935+2154. In the right panel, the gray circles illustrate the pointing of the 25 GRDs, the blue area represents the Earth shadow, the red circle indicates the 1σ location error of this burst, while the center of which is the best location, and the light blue line is the galactic plane (Huang et al. in the same journal).

Table 8
The Trigger Category of GECAM-B

Category	GRB	SGR J1935+2154	SGR J1555.2-5402	Uncertain	SFLARE	Particle Event	Occul.	Ins. Eff.a
Number	58	54	2	13	202	232	18	61
Percent (%)	9.1	8.4	0.3	2.0	31.6	36.3	2.8	9.5

Note.

Table 9
The Onboard Known Source Table

ID	Source Name	R.A. (deg)	Decl. (deg)	ON: 1 0FF: 0	HRª	Flux (erg/cm ² /s)	ER ^b (keV)
1	Solar	0	0	1	0-0.4	/	
2	/	0	0	0	0-0.4	,	,
3	,	0	0	0	0-0.4	,	,
4	,	0	0	0	0-0.4	/	,
5	,	0	0	0	0-0.4	/	,
6	Moon	0	0	1	0-0.4	/	,
7	CRAB	83.616	21.999	1	0-0.5	2.00E-08	3-17
8	GX 5-1	270.307	-25.086	1	0-0.4	1.98E-08	3-17
9	CIR X-1	230.152	-57.171	1	0-0.4	1.87E-08	3-17
10	GX 9+1	270.383	-20.52	1	0-0.4	1.45E-08	3-17
11	GX 349+2	256.429	-36.416	1	0-0.4	1.42E-08	3-17
12	GX 17+2	274.019	-14.015	1	0-0.4	1.22E-08	3-17
13	SCO X-1	244.979	-15.64	1	0-0.4	1.14E-08	17-60
14	CYG X-2	326.174	38.325	1	0-0.4	1.04E-08	3-17
15	GX 340+0	251.435	-45.623	1	0-0.4	9.06E-09	3-17
16	GX 13+1	273.625	-17.141	1	0-0.4	6.99E-09	3-17
17	GX 3+1	266.969	-26.572	1	0-0.4	6.37E-09	3-17
18	4U 1820-303	275.927	-30.374	1	0-0.4	4.73E-09	3-17
19	GX 9+9	262.934	-16.951	1	0-0.4	4.73E-09	3-17
20	GRO J1655-40	253.479	-39.836	1	0-0.4	4.65E-09	3-17
21	SER X-1	279.978	5.052	1	0-0.4	4.54E-09	3-17
22	4U 1636-536	250.207	-53.752	1	0-0.4	4.27E-09	3-17
23	GRS 1915+105	288.799	10.945	1	0-0.6	3.37E-09	17-60
24	A 0535+262	84.735	26.324	1	0-0.4	3.20E-09	17-60
25	CYG X-1	299.59	35.2	1	0-0.7	3.03E-09	100 - 150

^a Instrumental Effect.

Table 9 (Continued)

ID	Source Name	R.A. (deg)	Decl. (deg)	ON: 1 0FF: 0	HRª	Flux (erg/cm ² /s)	ER ^b (keV)
26	4U 1735-444	264.724	-44.467	1	0-0.4	3.03E-09	3-17
27	VELA X-1	135.529	-40.555	1	0-0.5	2.57E-09	17-60
28	4U 1700-377	255.985	-37.845	1	0-0.4	2.47E-09	17-60
29	GX 301-2	186.654	-62.772	1	0-0.4	2.21E-09	17-60
30	4U 1705-440	257.219	-44.13	1	0-0.4	2.09E-09	3-17
31	KS 1731-260	263.573	-26.088	1	0-0.4	1.95E-09	3-17
32	GX 354-0	262.984	-33.86	1	0-0.4	1.83E-09	3 - 17
33	4U0115+63	19.625	63.746	1	0-0.4	1.80E-09	17-60
34	CYG X-3	308.136	40.948	1	0-0.9	1.67E-09	17-60
35	XTE J1550-564	237.706	-56.484	1	0-0.4	1.53E-09	3-17
36	EXO 2030+375	308.062	37.638	1	0-0.4	1.27E-09	17-60
37	HER X-1	254.459	35.343	1	0-0.4	1.18E-09	17-60
38	4U 1901+03	285.917	3.207	1	0-0.4	1.15E-09	17-60
39	SWIFT J174510.8-262411	266.3	-26.4	1	0-0.4	1.14E-09	100 - 150
40	IGR J17544-2619	268.585	-26.335	1	0-0.4	1.13E-09	18-60
41	EXO 0331+530	53.75	53.173	1	0-0.4	1.12E-09	20 - 40
42	GS 1826-24	277.37	-23.798	1	0-0.5	1.06E-09	17-60
43	GRS 1758-258	270.308	-25.748	1	0-0.4	1.06E-09	18-60
44	4U 1624-490	247.001	-49.171	1	0-0.4	1.04E-09	3-17
45	GX 339-4	255.707	-48.79	1	0-0.4	1.02E-09	17-60
46	1E 1740.7-2942	265.977	-29.746	1	0-0.7	1.02E-09	18-60
47	GRO J0422+32	65.42	32.78	1	0-0.4	/	/

Table 10
The GRBs Triggered in-flight by GECAM-B

No.	Name	Short (0) Long (1)	Trigger Time (UTC)	R.A. (deg.)	Decl. (deg.)	Err (deg.)	TrigB (s)	TrigC
1	GRB 210120A	1	2021-01-20T07:10:48.550	151.37	55.27	3.19	4	1~5
2	GRB 210121A	1	2021-01-21T18:41:48.800	22.12	-49.51	1.25	0.1	$1\sim5$
3	GRB 210124A ^a	1	2021-01-24T11:50:03.600	102.97	27.2	3.1	4	$0 \sim 1$
4	GRB 210126A	1	2021-01-26T10:00:10.600	106.05	-56.26	6.1	4	$1\sim5$
5	GRB 210204A	1	2021-02-04T06:30:00.600	122.98	5.07	3.33	2	$1\sim5$
6	GRB 210207B	1	2021-02-07T21:52:50.550	253.74	61.85	1	2	3∼5
7	GRB 210228A	1	2021-02-28T06:38:32.600	85.58	-42.45	1.79	1	$1\sim5$
8	GRB 210307B	0	2021-03-07T05:56:39.100	125.6	17.5	7.3	0.5	3∼5
9	GRB 210317A	1	2021-03-17T09:08:28.550	157.06	-70.05	2.41	1	$1\sim5$
10	GRB 210330A	1	2021-03-30T12:45:46.600	168.89	-48.81	4.67	1	$1\sim5$
11	GRB 210328A	1	2021-03-28T20:45:17.900	198.32	-5.21	11.41	2	$1\sim5$
12	GRB 210401A	1	2021-04-01T23:21:14.350	269.56	-33.64	5.48	1	$1\sim5$
13	GRB 210409A	1	2021-04-09T21:28:07.950	69.4	-59.31	2.77	0.5	$1\sim5$
14	GRB 210413A	1	2021-04-13T01:07:25.600	68.62	11.25	3.64	2	$1\sim5$
15	GRB 210425A	0	2021-04-25T07:07:04.200	67.53	-51.76	2.73	0.2	$1\sim5$
16	GRB 210427A	1	2021-04-27T04:57:13.100	175.26	-59.87	5.75	0.2	$1\sim5$
17	GRB 210511B	1	2021-05-11T11:26:40.600	317.99	59.53	3.19	0.5	$1\sim5$
18	GRB 210516A	1	2021-05-16T23:34:46.550	332.4	66.97	1	0.2	$1\sim5$
19	GRB 210520A	1	2021-05-20T19:07:03.550	129.04	-72.01	5.55	1	$1\sim5$
20	GRB 210602B	1	2021-06-02T20:46:04.400	191.98	-54.42	24.48	4	$2\sim4$
21	GRB 210606B	1	2021-06-06T22:41:08.100	85.53	-16.49	1	0.5	$1\sim5$
22	GRB 210619B	1	2021-06-20T00:00:00.950	334.73	28.59	31	0.2	$1\sim5$
23	GRB 210622B	1	2021-06-22T10:33:02.600	123.92	-13.83	4.82	4	1~5
24	GRB 210627B	1	2021-06-27T17:57:21.550	235.3	0.61	3.6	1	1~5

Notes. a Hardness Ratio, with higher energy range of 25–250 keV, and lower energy range of 8–25 keV. b Energy Range of Flux.

Table 10 (Continued)

No.	Name	Short (0) Long (1)	Trigger Time (UTC)	R.A. (deg.)	Decl. (deg.)	Err (deg.)	TrigB (s)	TrigC
25	GRB 210719A	1	2021-07-19T02:24:59.500	73.79	50.7	3.98	4	1~5
26	GRB 210822A	1	2021-08-22T09:18:18.000	310.28	4.53	1	0.05	$1\sim5$
27	GRB 210827B	1	2021-08-27T10:10:16.600	305.31	-16.42	6.18	1	$1\sim 2$
28	GRB 210909B	1	2021-09-09T20:02:33.600	358.65	-74.92	1.08	2	$2\sim4$
29	GRB 210919A	0	2021-09-19T00:28:33.800	91.15	46.54	6.49	0.2	$1\sim5$
30	GRB 210923B	0	2021-09-23T02:11:29.150	238.558	-13.735	11.46	0.05	$1\sim5$
31	GRB 210925A	1	2021-09-25T19:12:34.600	357.83	-24.58	3.5	2	$1\sim2$
32	GRB 210926A	1	2021-09-26T20:52:28.250	351.51	-18.21	2.86	1	$1\sim2$
33	GRB 210927B	1	2021-09-27T23:54:45.600	240.27	69.51	9.85	2	$2\sim4$
34	GRB 211022A	1	2021-10-22T00:47:28.100	149.05	-57.56	3.15	1	$2\sim4$
35	GRB 211102B	1	2021-11-02T14:05:35.350	303.37	-4.61	2.79	0.5	1~5
36	GRB 211105A	1	2021-11-05T04:35:20.200	68.45	-67.97	2.56	2	$2\sim4$
37	GRB 211106A	0	2021-11-06T04:37:31.250	316.281	-48.185	19.48	0.1	$1\sim5$
38	GRB 211109C	1	2021-11-09T07:51:02.200	169.11	-61.78	8.17	1	$1\sim2$
39	GRB 211110A	1	2021-11-10T03:26:29.600	61.21	-29.49	4.21	2	$1\sim5$
40	GRB 211120A	1	2021-11-20T23:05:20.600	311.3	41.3	1.01	0.5	$1\sim5$
41	GRB 211204C	1	2021-12-04T21:37:00.250	332.78	52.66	2.22	1	$1\sim5$
42	GRB 211211B	1	2021-12-11T21:48:43.050	225.2	55.28	3.52	0.5	$1\sim5$
43	GRB 211216A	1	2021-12-16T06:45:56.050	57.22	-63.04	5.71	1	$1\sim5$
44	GRB 211216B	1	2021-12-16T13:21:08.550	106.24	45.53	5.78	4	$1\sim5$
45	GRB 211217A	1	2021-12-17T07:04:30.550	356.78	24.1	8.23	1	$0 \sim 1$
46	GRB 211223A	1	2021-12-23T02:41:18.900	316.04	-28.85	5.56	0.1	$1\sim5$
47	GRB 211229A	1	2021-12-29T03:30:05.200	302.74	27.58	8.72	2	$2\sim4$
48	GRB 211229B	1	2021-12-29T22:18:43.150	179.3	-25.09	2.85	0.5	$1\sim5$
49	GRB 211231A	1	2021-12-31T07:00:35.050	292.3	-5.78	2.73	1	$1\sim5$
50	GRB 220104A	1	2022-01-04T04:01:02.850	192.9	37.31	10.14	0.5	$1\sim5$
51	GRB 220121B	1	2022-01-21T02:07:37.100	48.45	-23.96	4.58	0.5	$1\sim5$
52	GRB 220124A	1	2022-01-24T03:37:38.200	246.16	42.29	2.96	2	$1\sim5$
53	GRB 220127A	1	2022-01-27T18:53:26.100	306.36	-44.3	5.14	0.5	$1\sim5$
54	GRB 220130A	1	2022-01-30T23:15:59.600	8.28	-54.8	8.89	4	$1\sim5$
55	GRB 220131B	1	2022-01-31T01:09:16.700	304.52	5.5	3.18	0.5	$1\sim2$
56	GRB 220203A	0	2022-02-03T21:15:39.750	314.27	11.16	5.99	0.05	$1\sim5$
57	GRB 220209A	1	2022-02-09T23:00:59.200	4.32	65.32	4.98	0.5	$1\sim5$
58	GRB 220310A	1	2022-03-10T00:28:17.250	169.34	14.93	2.6	1	$1\sim5$
59	GRB 220320A	1	2022-03-20T04:39:56.250	68.99	-47.4	3.42	4	$1\sim5$
60	GRB 220401B	1	2022-04-01T21:29:51.050	0.88	36.59	7.29	4	$1\sim 2$
61	GRB 220403B	1	2022-04-03T20:42:40.100	18.38	76.04	3.76	2	$0\sim 1$
62	GRB 220405A	1	2022-04-05T06:11:39.600	21.32	-24.27	4.06	0.5	$2\sim4$
63	GRB 220426C	0	2022-04-26T07:41:28.550	72.2	14.58	4.87	0.1	$2\sim4$
64	GRB 220511A	1	2022-05-11T13:41:56.800	286.78	15.26	1.28	0.5	$1\sim5$
65	GRB 220514A	1	2022-05-14T12:24:32.950	139.81	19.08	3.46	1	$1\sim5$
66	GRB 220521A	1	2022-05-21T23:20:22.100	276.41	8.78	6.48	0.5	$0\sim1$
67	GRB 220523B	1	2022-05-23T13:24:08.550	120.3	67.87	3.63	0.5	$1\sim 2$
68	GRB 220603A	1	2022-06-03T01:41:23.450	142.77	-39.48	6.26	4	$1\sim5$
69	GRB 220606C	1	2022-06-06T13:35:17.950	204.5	-7.56	3.58	0.1	$1\sim5$
70	GRB 220609B	1	2022-06-09T12:21:11.050	350.43	-1.26	5.51	1	$1\sim5$
71	GRB 220613A	1	2022-06-13T20:23:37.600	190.07	13.02	1.22	0.5	$1\sim5$
72	GRB 220620A	1	2022-06-20T01:32:05.050	95.81	60.33	5.16	2	$1\sim 2$
73	GRB 220623A	1	2022-06-23T07:04:10.650	157.94	75.69	9.24	0.1	$1\sim5$
74	GRB 220623B	0	2022-06-23T15:33:57.200	239.74	46.79	17.8	0.1	$2\sim4$
75	GRB 220624B	1	2022-06-24T10:20:25.550	91.42	36.44	4.47	1	$1\sim5$
76	GRB 220705A	0	2022-07-05T06:45:54.050	178.11	-40.06	5.91	1	$2\sim4$
77	GRB 220710A	1	2022-07-10T03:29:32.550	224.24	19.98	4.05	1	$1\sim 2$
78	GRB 220711C	0	2022-07-11T16:11:58.600	110.01	-55.8	5.72	0.1	$1\sim5$
79	GRB 220713A	1	2022-07-13T16:35:45.050	353.91	41.47	14.48	2	$1\sim 2$
80	GRB 220715A	1	2022-07-15T08:49:40.450	177.91	-26.71	26.66	0.2	$1\sim5$

Note. $^{\rm a}$ X-ray burster 4U 0614+09 or GRB 210124A.

demonstrated for the first time that the novel application of BeiDou short messages to transmit astronomical alerts (trigger information) from satellite to ground is very successful, and the time latency of the first short message of a trigger is about 1 minute, much better than expectation before launch. Figure 11 shows the light curve of the first long trigger received via BDS-3. Figure 12 displays the high time resolution light curve (left panel) and the in-flight localization (right panel) for the first short trigger. The high time resolution light curve is used to provide a more accurate location of GRBs with the time-delay localization method once the data from several spacecraft are downlinked to the ground (Xiao et al. 2021).

Table 10 lists the GRBs and X-ray bursts from XRBs triggered in-flight with precise location. The location offset distribution is analyzed in Huang et al. in the same journal. The categories of in-flight triggers are analyzed based on data from 2021-08-01T00 to 2022-08-01T00 UTC. During this time period, there are a total of 4879 triggers from GECAM-B; 84.03% of them are Type II triggers and 15.97% are Type I. Among these 779 Type I triggers, excluding 139 false triggers due to higher temperatures and SiPM noise, the ground reclassification of the remaining 640 triggers is shown in Table 8, of which ∼18% are from GRBs and SGRs.

6. Discussion and Conclusion

We developed a dedicated onboard trigger and localization software running on a microcontroller unit (CPU) of GECAM EBox. It can not only trigger and localize various bursts, but also can classify whether the burst is long or short, and judge whether the burst is valuable (Type I trigger) or not (Type II trigger). For valuable triggers, it can generate trigger information that could be transmitted to the ground in near realtime with the GSMC service of the BeiDou navigation system. The time latency of the first short message for in-flight trigger is about 1 minute, and short messages of nearly all triggers can be received in about 10 minutes. Based on the on-ground tests and in-flight performances, this software successfully achieves the design goal.

Acknowledgments

The GECAM (Huairou-1) mission is supported by the Strategic Priority Research Program on Space Science of the Chinese Academy of Sciences. The authors thank the support from the Strategic Priority Research Program on Space Science (grant Nos. XDA15360300, XDA15360000, XDA15360102,

XDA15052700 and E02212A02S) of the Chinese Academy of Sciences, the National Natural Science Foundation of China (NSFC, Grant No. 12173038) and BeiDou navigation system. We would also like to thank the referee for carefully reading and valuable comments and suggestions, which have significantly improved the quality of this manuscript.

ORCID iDs

Qi Luo https://orcid.org/0000-0003-1853-7810

Jin-Yuan Liao https://orcid.org/0000-0001-8277-6133

Yue Huang https://orcid.org/0000-0002-3515-9500

Can Chen https://orcid.org/0000-0001-7210-3461

Rui Qiao https://orcid.org/0000-0001-7398-0298

Li-Ming Song https://orcid.org/0000-0003-0274-3396

Feng Shi https://orcid.org/0000-0002-7491-5188

References

```
An, Z. H., Sun, X. L., Zhang, D. L., et al. 2022, RDTM, 6, 43
Aptekar, R. L., Frederiks, D. D., Golenetskii, S. V., et al. 1995, SSRv, 71, 265
Cai, C. 2022, Observational Studies of Short Time-Scale High-Energy Bursts,
   Doctoral Dissertation, Institute of High Energy Physics, CAS
Chen, C., Xiao, S., Xiong, S., et al. 2021, ExA, 52, 45
Chen, W., Li, B., Huang, Y., et al. 2020, SSPMA, 50, 129512
Dong, Y., Wu, B., Li, Y., Zhang, Y., & Zhang, S. 2010, SCPMA, 53, 40
Gehrels, N., Chincarini, G., Giommi, P., et al. 2004, ApJ, 611, 1005
Godet, O., Nasser, G., Atteia, J., et al. 2014, Proc. SPIE, 9144, 914424
Guo, D., Peng, W., Zhu, Y., et al. 2020, SSPMA, 50, 129509
HAN, X., ZHANG, K., HUANG, J., et al. 2020, SSPMA, 50, 129507
Hurley, K., Pal'shin, V. D., Aptekar, R. L., et al. 2013, ApJS, 207, 39
Jin-Yuan, L., Qi, L., Yue, Z., et al. 2020, SSPMA, 50, 129510
Li, C., Peng, W., Xu, Y., et al. 2022, NIMPA, 1022, 165969
Li, G., Guo, S., Lv, J., Zhao, K., & He, Z. 2021, AdSpR, 67, 1701
LI, X., WEN, X., AN, Z., et al. 2020, SSPMA, 50, 129508
Liu, Y. Q., Gong, K., Li, X. Q., et al. 2022, RDTM, 6, 70
Lv, P., Xiong, S., Sun, X., Lv, J., & Li, Y. 2018, JInst, 13, P08014
Marrocchesi, P. S. 2018, in The Fourteenth Marcel Grossmann Meeting On
   Recent Developments in Theoretical and Experimental General Relativity,
   Astrophysics, and Relativistic Field Theories, ed. M.
   R. T. Jansen, & R. Ruffini (Singapore: World Scientific), 3315
Meegan, C., Lichti, G., Bhat, P. N., et al. 2009, ApJ, 702, 791
Mereghetti, S., Götz, D., Borkowski, J., Walter, R., & Pedersen, H. 2003,
   A&A, 411, L291
Rao, A. R., Chand, V., Hingar, M. K., et al. 2016, ApJ, 833, 86
Saraogi, D., Balasubramanian, A., Mate, S., et al. 2022, in 44th COSPAR
   Scientific Assembly, 2255
Sharma, Y., Marathe, A., Bhalerao, V., et al. 2021, JApA, 42, 73
Xiao, S., Xiong, S. L., Zhang, S. N., et al. 2021, AJ, 920, 43
Xu, Y. B., Li, X. Q., Sun, X. L., et al. 2022, RDTM, 6, 53
Yuan, W., Zhang, C., Chen, Y., et al. 2018, SSPMA, 48, 039502
Zhang, C., Liang, X., Xu, Y., et al. 2022, RDTM, 6, 26
Zhang, D., Li, X., Xiong, S., et al. 2019, NIMPA, 921, 8
Zhang, S.-N., Li, T., Lu, F., et al. 2020, SCPMA, 63, 249502
```